

Nonlinear exchange coupling and magnetic domain asymmetry in ferromagnetic/IrMn thin films

Jeffrey McCord,^{*} Christine Hamann, Rudolf Schäfer, and Ludwig Schultz
Institute for Metallic Materials, IFW Dresden, Postfach 270116, 01171 Dresden, Germany

Roland Mattheis

Institute of Photonic Technology, Albert-Einstein-Strasse 9, 07745 Jena, Germany

(Received 26 July 2008; revised manuscript received 19 August 2008; published 19 September 2008)

Noncollinear uniaxial and unidirectional exchange anisotropy contributions are discovered and identified as a cause of loop asymmetry in exchange-coupled ferromagnetic/antiferromagnetic thin films. Adjusting the magnetic reversal field axis to compensate for the tilted anisotropies eliminates the loop and magnetic domain reversal asymmetry. The deviation from collinearity of exchange coupling is suggested to originate from antiferromagnetic-layer-induced interfacial magnetic frustration. The effects are independent of the occurrence of exchange bias, existing below and above the onset of exchange bias. The additional anisotropy contributions add another mechanism to the occurrence of exchange coupling.

DOI: [10.1103/PhysRevB.78.094419](https://doi.org/10.1103/PhysRevB.78.094419)

PACS number(s): 75.60.-d, 75.70.-i

I. INTRODUCTION

Exchange interaction at the interfaces of layered ferromagnetic (FM) and nonmagnetic (NM) or antiferromagnetic (AF) films is a major contribution to the effective magnetic properties of thin-film nanostructures. In particular, exchange coupling across a NM transition-metal layer is observed in FM/NM/FM sandwich structures. There, the sign of coupling depends on the NM layer thickness and may result in a preferred parallel, respectively, antiparallel alignment of the spins of the FM layers in the magnetic ground state.^{1,2} For certain materials systems a biquadratic coupling,³⁻⁵ favoring an orthogonal orientation of magnetization, becomes the dominating contribution. It may originate from local thickness variations, which result in spatial fluctuations of the bilinear interlayer coupling terms, inhomogeneities of the interlayer spin structure, FM impurities in the NM interlayer matrix, or magnetic proximity effects. On the other hand, direct exchange coupling is used to control the magnetic properties in exchange spring hard/soft FM/FM (Ref. 6) or exchange biased FM/AF bilayers.⁷ In the FM/FM systems the FM layers are accessible to traditional magnetic measurement techniques and it has been shown that by introducing a fluctuating spin structure in the FM hard layer, an effective biquadratic coupling across the interface is introduced.⁸⁻¹⁰

For exchange biased systems, however, the magnetization of the AF layer can neither be adjusted nor probed easily. In such systems a stabilization of the FM magnetization along a preferred direction is achieved by the exchange bias effect, which for FM/AF structures manifests itself in a ferromagnetic loop shift^{7,11-14} after the setting of unidirectional anisotropy during film deposition or by a field cooling process. Various possible coupling mechanisms have been proposed to describe the exchange effect in agreement with experimentally obtained data.¹⁵⁻¹⁸ Biquadratic or spin-flop coupling across the FM/AF layer has been proven to exist in single-crystalline FeF₂-based systems with well-defined and high uniaxial AF anisotropy.¹⁹ The occurrence of positive exchange bias in such systems²⁰ has been found to depend on the magnitude of the applied magnetic field²¹ during the field cooling process. For polycrystalline FM/AF layers, where

the in-plane AF anisotropy axes of the grains are equally distributed,²² the existence of pinned uncompensated spins at the interface is found to be responsible for the exchange bias effect.²³ For such systems, applying a magnetic field H_{dep} during AF film deposition on top of a saturated FM layer predominately results in an exchange bias field H_{eb} or unidirectional anisotropy $K_{\text{ud,FM-AF}}$ along and parallel to the initially applied magnetic-field direction.

In addition, exchange biased FM/AF systems evidence loop asymmetry effects,²⁴⁻²⁷ which are explained by irreversible magnetization processes in the antiferromagnetic layer^{25,28} or by a misaligned external magnetic field^{28,29} during reversal of an otherwise collinear coupled FM/AF system. In the latest coherent rotation models the reversal depends strongly on the ratio between FM film uniaxial anisotropy and unidirectional anisotropy.³⁰ Yet, the proposed models are not able to explain all aspects of the symmetry breaking phenomena. Especially, asymmetric ferromagnetic domain formation and incoherent rotation processes,^{25,31-33} where the magnetic switching field is aligned along the expected direction of exchange bias, are not understood. In this paper we show evidence for the existence of tilted uniaxial and unidirectional exchange anisotropies, deviating from collinearity, in FM/AF systems, which lead to asymmetric magnetization reversal phenomena.

II. EXPERIMENT

To investigate the asymmetry effects, Ta(5 nm)/FM(20 nm)/Ir₂₃Mn₇₇/Ru(3 nm) (FM=Co₉₀Fe₁₀ or Ni₈₁Fe₁₉) films with varying AF thickness ($t_{\text{IrMn}}=0-9$ nm) were prepared by dc-magnetron sputtering on Si/SiO₂ substrates. The Ta-seed layer ensures a $\langle 111 \rangle$ -fiber texture of the polycrystalline films^{22,25} and no signs of in-plane texture were detected.²² The uniaxial anisotropy $K_{u,\text{FM}}$ of the FM layer and the unidirectional anisotropy $K_{\text{ud,FM-AF}}$ transmitted from the AF layer grown on top of the FM layer were set in a magnetic in-plane field of $H_{\text{dep}}=4.0$ kA/m during the FM and AF film deposition. By this procedure an exact parallel alignment of the uniaxial anisotropy of the FM

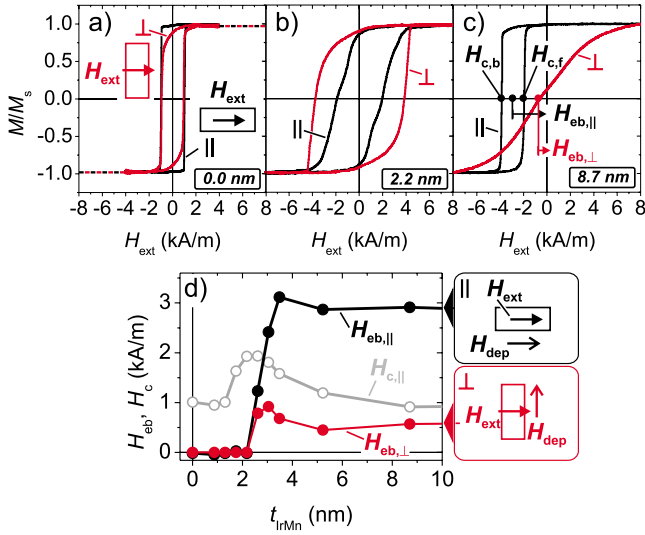


FIG. 1. (Color online) (a)–(c) Magnetization loops for CoFe(20 nm)/IrMn magnetic bilayers measured along (||) and perpendicular (⊥) to H_{dep} . The AF-layer thicknesses t_{IrMn} are indicated. The positions of the backward $H_{c,b}$ and forward $H_{c,f}$ coercivities are displayed in (c). The values of $H_{c,||}$, $H_{c,⊥}$ and bias field $H_{eb,⊥}$ along the perpendicular direction vs t_{IrMn} are plotted in (d). The directions of field and the sample orientation are defined in (d).

and the imprinted exchange bias field direction ($K_{\text{ud,FM-AF}} \parallel K_{u,\text{FM}}$) was intended. The magnetic properties were characterized by inductive magnetometry at 10 Hz and the magnetic domains were probed by magneto-optical Kerr effect microscopy.³⁴ Both methods allow a precise adjustment of the sample’s orientation with direct feedback to corresponding changes in the magnetization behavior. All hysteresis loops were obtained in a trained state after at least 50 magnetization loops in order to minimize effects from irreversible changes in the AF-layer magnetization and other related magnetic history effects.

III. RESULTS

A. Magnetization reversal along and perpendicular to H_{dep}

Magnetization loops for the CoFe samples with different IrMn layer thickness measured exactly parallel (||) and perpendicular (⊥) to the *deposition field direction* (indicated as being || to the elongated side of the samples) are displayed in Fig. 1. With increasing AF-layer thickness the coercivity field increases and peaks around $t_{\text{IrMn}}=2.2$ nm. For the ||-case the loop shape changes significantly from a rather square shaped easy axis [Fig. 1(a)] to a tilted loop that resembles a hard axis loop [Fig. 1(b)]. Congruently, the ⊥-loop displays signatures of an easy axis loop, which manifests itself in higher coercivity values and larger squareness of the ⊥-loop relative to the ||-loop. This indicates an AF-layer-induced rotation of the effective uniaxial anisotropy direction. With further increasing t_{IrMn} , the bilayers exhibit a loop shift along the ||-direction ($H_{eb,||}$). Yet, the ⊥-loops display a noticeable exchange bias field $H_{eb,⊥}$. This field offset is unexpected and points to a rotated exchange bias field direction that is misaligned relative to the deposition field

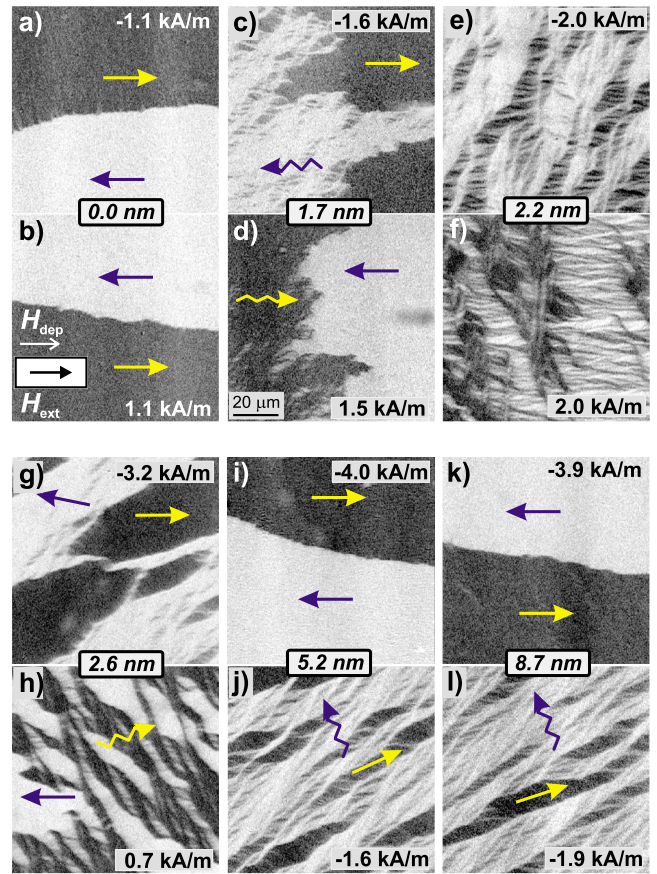


FIG. 2. (Color online) Magnetic domain structures in CoFe(20 nm)/IrMn obtained at $H_{c,b}$ and $H_{c,f}$ displaying asymmetric magnetization reversal. The applied field H_{ext} was oriented parallel to H_{dep} . The sample orientation for all measurements is displayed in (b). t_{IrMn} and the values of H_{ext} are indicated. Directions of net magnetization are sketched.

direction H_{dep} . A similar behavior originating from a misalignment between the easy axis of ferromagnetic and anti-ferromagnetic films in exchange biased MnPt/NiFe bilayers, where the AF layer was deposited prior to FM layer deposition, has been discussed in Ref. 35.

Complementary magnetic domain images obtained at the coercive fields $H_{c,b}$ and $H_{c,f}$ for the backward and forward loop branches are displayed in Fig. 2. Whereas the reversal for the pure CoFe films [Figs. 2(a) and 2(b)] proceeds symmetrically through 180-deg domain-wall motion, irregular and asymmetric domain characteristics are observed with the addition of the AF layer. The change in magnetic microstructure with the addition of IrMn and below the onset of exchange bias is shown for two different AF thicknesses in Figs. 2(c)–2(f). With the addition of IrMn a transition to a more nonuniform or dispersive magnetic domain pattern takes place, which indicates AF-induced magnetic disorder in the FM layer. Magnetization modulated domains with the net magnetization oriented nearly perpendicular to H_{ext} and H_{dep} for $t_{\text{IrMn}}=2.2$ nm become visible. This finding confirms the assumption of a rotated effective anisotropy axis. For larger AF-layer thickness, the reversal process displays a pronounced asymmetry in magnetic domain formation [Figs.

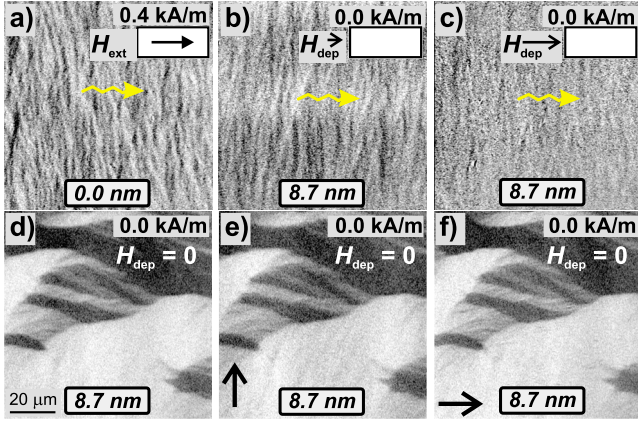


FIG. 3. (Color online) Magnetic domain structures in CoFe(20 nm) and CoFe(20 nm)/IrMn films obtained for different deposition and external field history. For the FM (a) and FM/AF structures (b) and (c) the deposition field was varied from (a) $H_{\text{dep}}=0$ kA/m and (b) $=0.1$ kA/m up to (c) $=0.4$ kA/m. For (d)–(f) $H_{\text{dep}}=0$ kA/m while the magnetic history before domain imaging was varied (see text for details). The directions of net magnetization are sketched in (a)–(c). The sample orientation and the values of H_{ext} are indicated.

2(g)–2(l)]. The magnetization process occurs by domain-wall propagation for the backward and by incoherent magnetization rotation and domain-wall motion for the forward loop branch.^{25,33}

For the correct interpretation of the experiments a perfectly controlled alignment of the magnetic-field direction during deposition is essential. The direction of magnetic field was probed *after* film preparation on selected samples by analysis of the rippled magnetization structure, which occurs in polycrystalline FM thin-film samples.^{34,36} An example of the domain structure of a pure FM CoFe layer in an applied magnetic field under similar conditions as during film deposition, $H_{\text{ext}} \approx H_{\text{dep}}$, is displayed in Fig. 3(a). A saturated homogeneous magnetic structure with the magnetization mainly aligned along H_{ext} is expected from the magnetization loops [see Fig. 1(a)]. However, due to FM anisotropy dispersion a small modulation of magnetization occurs, the orientation of which is constrainedly aligned perpendicular to the direction of mean magnetization and therefore a direct measure of the alignment of field. On the other hand, a magnetization pattern or the FM domain structure during subsequent AF film deposition is assumed to directly transfer into a pattern of exchange bias, where the direction of H_{eb} mimics the FM domain pattern. A typical example of a magnetic domain structure obtained in a CoFe/IrMn film deposited in the absence of a deposition field ($H_{\text{dep}}=0$ kA/m) is displayed in Fig. 3(d). The domain structure is fixed by local exchange bias and reproduces reversibly at remanence after applying a field of $H_{\text{ext}}=80$ kA/m perpendicular [\uparrow , Fig. 3(e)] and along [\rightarrow , Fig. 3(f)] for more than 1 h. Consequently, the domain structure during film deposition is permanently imprinted and the FM/AF domain structure reflects the FM magnetic state during AF film deposition. The remanent FM magnetic structures for two different amounts of H_{dep} are displayed in Figs. 3(b) and 3(c). For both field amplitudes a modulated magnetic structure similar to Fig. 3(a)

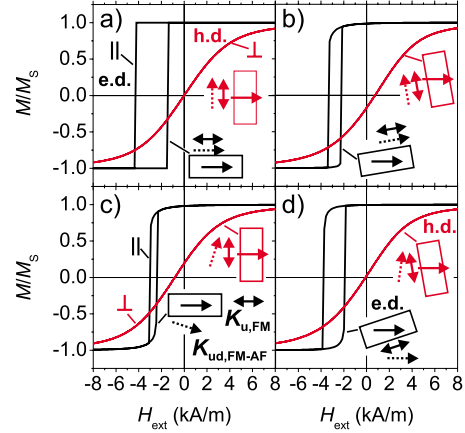


FIG. 4. (Color online) Modeled magnetization loops for a magnetic bilayer structure measured under different angles α relative to the exchange bias direction. $K_{u,\text{FM}}=740$ J/m³ and $K_{\text{ud,FM-AF}}=1 \times 10^{-4}$ J/m² in accordance with Fig. 1(d) were used for the calculations. The saturation polarization $J_s=1.9$ T was determined from measuring the saturation field perpendicular to the film plane. The sample orientation, respectively the direction of $K_{u,\text{FM}}$ and $K_{\text{ud,FM-AF}}$ are indicated [defined in (c)].

becomes visible. The amplitude of magnetic ripple is less than 3° as derived from magnetic contrast analysis and more pronounced for the case of reduced deposition field amplitude H_{dep} in Fig. 3(b). Importantly, the engraved domain modulation patterns are oriented perpendicular to the intended direction of H_{dep} and validate that the direction of H_{dep} is along the presumed direction. For the magnetically more soft NiFe-based FM/AF sample no ripple domain structures were found. By the presented *ex situ* experiments the true direction of deposition field is evidenced.

B. Phenomenology of AF-induced tilted anisotropy effects

The fundamental correlation of the magnetization behavior with canted anisotropy for the case of a thick AF layer, similar to the situation in Fig. 1(c), is demonstrated by modeling the hysteresis loop, e.g., minimizing the total areal energy density e_{tot} relative to the direction of magnetization θ given by

$$e_{\text{tot}} = K_{u,\text{FM}} t_{\text{FM}} \sin^2(\alpha - \theta) - K_{\text{ud,FM-AF}} \cos(\beta - \theta) - H_{\text{ext}} J_s t_{\text{FM}} \cos(\gamma - \theta), \quad (1)$$

with the ferromagnetic uniaxial anisotropy energy density $K_{u,\text{FM}}$ aligned along α , the unidirectional exchange anisotropy $K_{\text{ud,FM-AF}}$ oriented with β , and the external field H_{ext} in direction of γ . Calculated easy and hard axis loops for different angular conditions are shown in Fig. 4. The loops for parallel alignment of field and anisotropy axis (||, e.d.: $\alpha=\beta=\gamma=0$; \perp , h.d.: $\alpha=\beta=\pi/2$, $\gamma=0$) and tilting the sample ($\alpha=\beta=0.17$, $\gamma=0$ and $\alpha=\beta=\pi/2+0.17$, $\gamma=0$) are shown in Figs. 4(a) and 4(b). As discussed above, a tilt of the unidirectional anisotropy direction leads to an effective loop shift $H_{\text{eb},\perp}$ despite the alignment of H_{ext} along H_{dep} . This situation is modeled in Fig. 4(c) (||: $\alpha=0$, $\beta=0.30$, $\gamma=0$; \perp : $\alpha=\pi/2$, $\beta=\pi/2+0.30$, $\gamma=\pi/2$). The bias field $H_{\text{eb},\perp}$ is com-

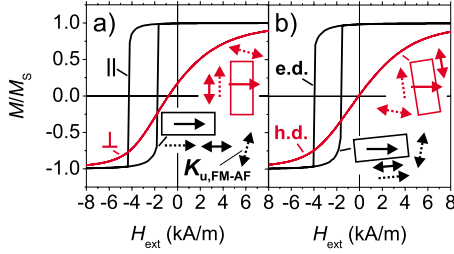


FIG. 5. (Color online) Modeled magnetization loops for a magnetic bilayer structure measured under different angles α under the assumption of a tilted AF-induced uniaxial anisotropy contribution $K_{u,FM-AF}=0.6 \times 10^{-4} \text{ J/m}^2$. The same values of $K_{u,FM}$ and $K_{ud,FM-AF}$ as in Fig. 4 were used for the modeling. The sample orientation, respectively the direction of $K_{u,FM}$, $K_{ud,FM-AF}$, and $K_{u,FM-AF}$ are indicated (cf. Fig. 4).

compensated by rotating the sample to 0.17 away from the ideal h.d. case as shown in Fig. 4(d). Due to the superposition of $K_{ud,FM-AF}$ and $K_{u,FM}$ this angle is less than the misalignment $\beta - \alpha = 0.30$. A symmetric loop is obtained for $\gamma = 0.28$ close to the direction of $K_{ud,FM-AF}$.

Alternatively, an AF-induced canted uniaxial anisotropy contribution would generate similar results. This is demonstrated by the modeled hysteresis loops in Fig. 5. For the calculation an energy landscape similar to Eq. (1) is assumed, yet an additional and possibly tilted uniaxial anisotropy term $K_{u,FM-AF}$ is introduced. The total energy density e_{tot} relative to the direction of magnetization is then given by

$$e_{tot} = K_{u,FM} t_{FM} \sin^2(\alpha - \theta) + K_{u,FM-AF} \sin^2(\delta - \theta) - K_{ud,FM-AF} \cos(\alpha - \theta) - H_{ext} J_s t_{FM} \cos(\gamma - \theta), \quad (2)$$

with, both, $K_{u,FM}$ and $K_{ud,FM-AF}$ being parallel and aligned along α and $K_{u,FM-AF}$ aligned along δ . Calculated loops along the direction of $K_{u,FM}$ and $K_{ud,FM-AF}$ and under the compensating conditions similar to Figs. 4(c) and 4(d) are shown in Fig. 5. An AF-induced interfacial uniaxial anisotropy coupling aligned nearly perpendicular to the deposition field direction, $\delta = 1.40$, was used for the modeling of the loops. As demonstrated in Fig. 5(b), the residual bias field $H_{eb,\perp}$ for the chosen parameters is compensated rotating the sample by 0.16 relative to the initially assumed hard direction and a symmetric loop is obtained for a rotation of 0.10 relative to the assumed e.a. direction of Fig. 5(a).

The above performed analysis is consistent with the existence of a tilted uniaxial or unidirectional anisotropy relative to the deposition field as suggested from the experimental results shown in Sec. III A. A clear distinction of both mechanisms is not easy, but the assumption of noncollinear AF-induced anisotropy contributions is consistent with the modeled noncollinear AF-induced anisotropy contributions. Whereas the single domain analysis is valid for the zero coercivity h.d. case, the results of the analysis along the e.d., with the existence of magnetic domains and incoherent reversal processes, is only able to give guidance to the understanding of the underlying reversal process.

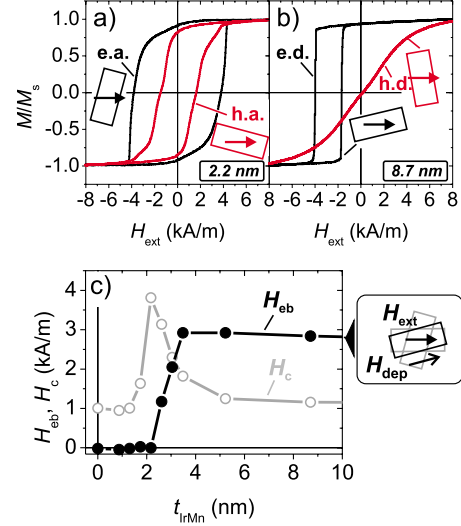


FIG. 6. (Color online) Exemplary magnetization loops for (a) CoFe(20 nm)/IrMn(2.2 nm) and (b) CoFe(20 nm)/IrMn(8.7 nm) magnetic bilayer structures measured along and perpendicular to the effective exchange bias direction as discussed in Fig. 4. The sample alignment for each measurement is indicated. H_c and H_{eb} as a function of t_{IrMn} are displayed in (c).

C. Compensating for asymmetry effects

Magnetization loops for $t_{IrMn} = 2.2 \text{ nm}$ and $t_{IrMn} = 8.7 \text{ nm}$ under the symmetric reversal conditions described above are displayed in Figs. 6(a) and 6(b). Comparing the loops of Figs. 1(c) and 6(b) to the calculated loops of Figs. 4 and 5, the general trends in the change in magnetization reversal are reproduced. Aligning the external field with the effective easy direction has only minor influence on the loop shift; only the coercivity increases significantly as can be seen comparing Fig. 1(d) with Fig. 6(c).

Investigating the domain formation along the effective easy axis [Fig. 6(a)] and effective easy direction [Fig. 6(b)], the domain structures display no more signs of asymmetry. In accordance with the presented analysis, the domain characteristics for the backward and forward loop are fundamentally identical. For thin IrMn layers [Figs. 7(a) and 7(b)] the magnetization is initialized by incoherent rotation under the formation of ripplelike domains. Remarkably, for thin AF layers residual effects from the FM's uniaxial anisotropy direction become directly visible in the orientation of low angle domain walls, which are aligned in parallel with H_{dep} , identical with $K_{u,FM}$. This is an additional and conclusive evidence of the coexistence of mixed and tilted FM- and AF-induced uniaxial anisotropy contributions. For thick AF layers, the reversal process now also occurs symmetric, yet, through domain-wall motion without signs of incoherent magnetization rotation. Similar data as shown in Figs. 7(e)–7(h) are obtained over the whole thickness range from $t_{IrMn} = 3.6$ to 8.7 nm. Aligning H_{ext} along the effective easy direction, compensating for the tilted orientation of anisotropies, eliminates loop and domain asymmetry effects. Only in the intermediate IrMn thickness range just above the onset of exchange bias [Figs. 7(c) and 7(d)] is a difference in the reversal modes for the forward and backward loop branches still evident.

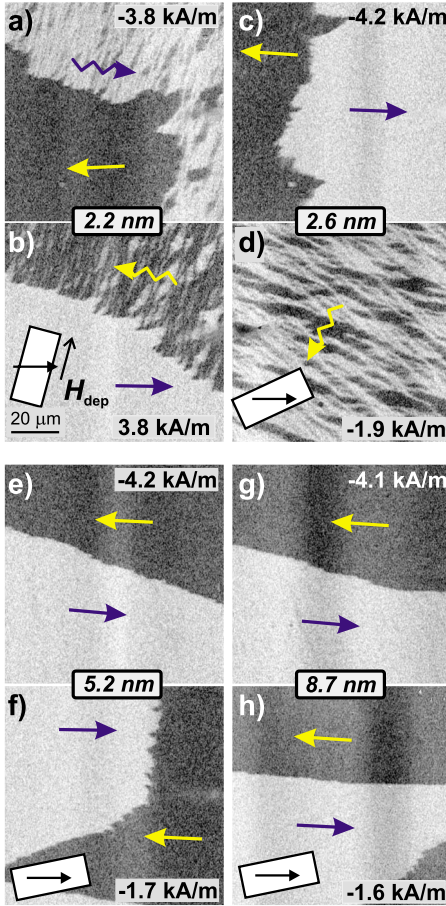


FIG. 7. (Color online) Magnetic domain structures in CoFe/IrMn layers obtained at $H_{c,b}$, respectively $H_{c,f}$. The applied magnetic field H_{ext} was oriented parallel to the effective uniaxial anisotropy axis (a), respectively effective exchange bias direction (b) (see Fig. 6). The direction of H_{dep} , the values of H_{ext} , and t_{IrMn} are indicated.

The anisotropy tilt is not restricted to CoFe/IrMn layers, but also appears in $Ni_{81}Fe_{19}/IrMn$ structures. Examples for a single-layer NiFe and bilayer NiFe/IrMn structures are displayed in Fig. 8. A well-defined uniaxial anisotropy loop is derived from the pure FM's magnetization loops, which are consistent with a FM uniaxial anisotropy $K_{u,FM}$ aligned along H_{dep} . With the addition of the IrMn layer [$t_{IrMn}=2.2$ nm, Fig. 8(b)] magnetization loops without a signature of anisotropy are found for the \parallel , respectively \perp loop case. As shown in Fig. 8(d), rotating the sample in accordance with a tilted AF-induced uniaxial anisotropy, magnetization loops similar to regular easy and hard axis loops are found. Furthermore, for thicker IrMn thicknesses a residual exchange bias field as for the CoFe-based sample is seen [Fig. 8(c)]. $H_{eb,\perp}$ is eliminated by rotating the sample away from the direction perpendicular to H_{dep} as shown in Fig. 8(e). The results indicate that the occurrence of AF-induced and titled anisotropies is independent of the FM material.

IV. DISCUSSION

In principle the observed tilted exchange bias could also be attributed to magnetic history dependent reorganization

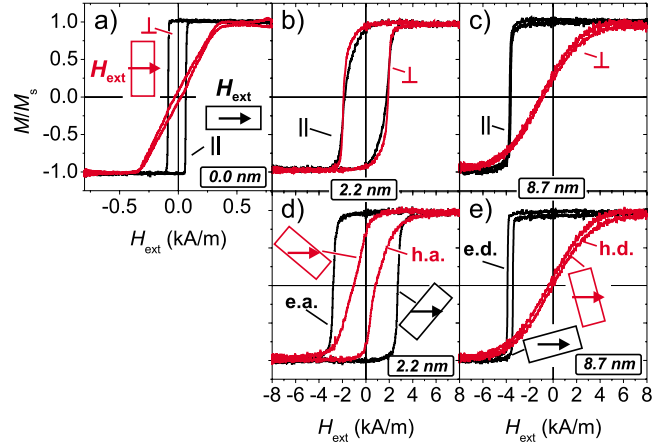


FIG. 8. (Color online) (a)–(c) Magnetization loops for $Ni_{81}Fe_{19}(20$ nm)/IrMn magnetic bilayers measured along (\parallel) and perpendicular (\perp) to H_{dep} . The hysteresis loops along and perpendicular to the effective easy (e.a.) and hard axis (h.a.) and direction (e.d., h.d.) of magnetization are shown in (d) and (e). The sample alignment for the measurements in (a)–(c) is sketched in (a); the orientations under the compensation conditions are displayed in (d) and (e).

processes of AF grain magnetization or AF domains. Irreversible switching process could lead to strong changes in the initial loops, depending on the angular field history.³⁷ A pronounced angular hysteresis for the initial (untrained) loops was also observed in Ref. 38. Even though in the experiments presented here the systems are investigated in a trained state and the behavior has been proven to be reproducible, the stability of anisotropy tilting versus magnetic-field history was investigated by comparing the magnetization behavior after a counterclockwise (ccw) field rotation to the behavior of a subsequent clockwise (cw) field rotation.

Results for the CoFe-based FM/AF layers are presented in Fig. 9. Shown in Figs. 9(a) and 9(b) are the final e.a. loops, respectively, and in Figs. 9(e) and 9(f) the final e.d. and h.d. loops after subsequent ccw-cw sample rotation in an alternating measurement field together with the change in magnetization loop behavior Δ after ccw to cw rotation. Neither for $t_{IrMn}=2.2$ nm nor for $t_{IrMn}=8.7$ nm a significant change in the loop behavior is detected. The general statements made above regarding the occurrence of tilted anisotropies are still valid after performing the rotational experiments. Only for the intermediate thicknesses, slightly above the onset of exchange bias [Figs. 9(c) and 9(d)], significant alterations in the differential loop behavior are detected. Along the e.d. a significant change in coercivity results in distinct peaks around H_c , which are more pronounced for the forward loop branch. From the measured change in magnetization loops, it becomes clear that an additional contribution from rotation processes in the partly unstable AF layer potentially plays a part in the tilted anisotropy effect and contributes in the still observable domain asymmetry shown in Figs. 7(c) and 7(d). Still, the measured contributions are well below the experimentally derived tilting angle of up to $\pi/2$ below the onset of exchange bias.

The overall change in misalignment of uniaxial anisotropy relative to the expected angle from the deposition field

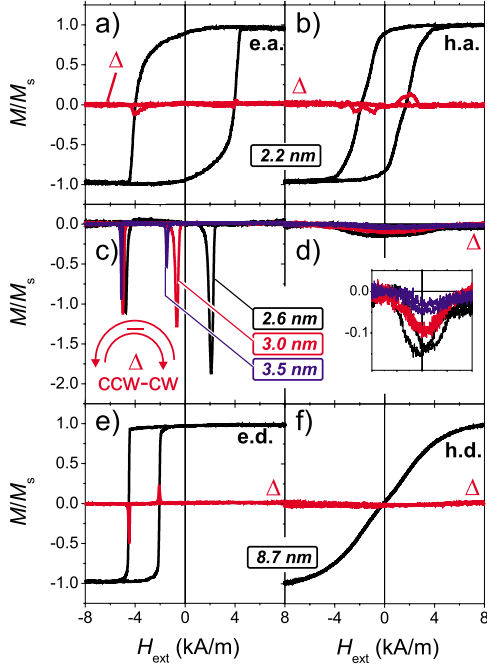


FIG. 9. (Color online) Change in easy and hard axis magnetization loop behavior with magnetic-field history. In (a)–(f) the measured difference in the magnetization loop after a ccw rotation of the sample and a cw rotation is displayed for several IrMn thicknesses. Examples of magnetization loops are displayed in (a) and (b), as well as in (e) and (f).

direction, respectively the misalignment angle under which a zero loop shift ($H_{\text{cb},\perp}=0$) is observed, is displayed in Fig. 10(a) for three different sets of CoFe- and NiFe-based FM/AF structures. Close to the onset of exchange bias the misalignment reaches values up to $\pi/2$, which drops significantly with increasing thickness of the AF layer but never reaches zero. For both CoFe and NiFe, a similar dependence on AF thickness is observed.

The exchange bias effect relies on a low fraction of pinned interfacial spins laterally distributed at the FM-AF interface,^{23,39} resulting in a magnetically inhomogeneous interface, where also chemical intermixing effects and magnetic proximity effects play a role.⁴⁰ Moreover, the stability of AF magnetization and AF domains contribute to the magnetic behavior.^{41,42} Due to the complexity of the FM-AF interaction, a complete theoretical analysis of the interfacial contributions is beyond the scope of this paper. The following discussion will therefore concentrate on the AF thickness around the onset of exchange bias, where the maximum of anisotropy tilt is observed. Reconsidering possible mechanisms for perpendicularly aligned effective anisotropies,^{5,8–10} the occurrence of biquadratic coupling is related to a spatially alternating sign of effective exchange coupling. This situation occurs, if the AF grain volume V_{AF} , in connection with anisotropy energy, is not large enough to achieve thermal stability at room temperature.^{42,43} This behavior dominates below the onset of exchange bias, where partial switching of AF grains occurs. The existence of such a behavior in IrMn-based FM/AF bilayers has been confirmed from measurements of the effective exchange bias by magnetization

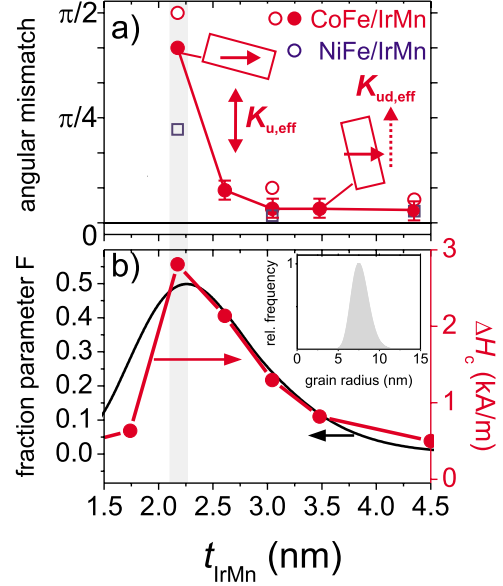


FIG. 10. (Color online) (a) Misalignment of the direction of uniaxial anisotropy $K_{\mu,\text{eff}}$ or effective easy direction $K_{\text{ud,eff}}$ relative to H_{dep} as derived from the zero loop shift condition for three different series of CoFe/IrMn and NiFe/IrMn thin films. (b) Calculated AF-layer dependence of fraction parameter $F = \sqrt{f^2(1-f)^2}$ derived from the fraction f of stable AF grains. The increase in coercivity ΔH_c relative to the FM film versus t_{IrMn} is added in (b). The inset in (b) shows the assumed log-norm distribution of grain radius used for the calculations.

dynamics.⁴¹ An equally divided fraction $f=0.5$ of stable and unstable AF grains is anticipated for an AF-layer thickness t_{IrMn} , where the condition^{42–44}

$$\frac{\Delta E}{k_B T} = \frac{K_{\text{AF,IrMn}} V_{\text{AF}}}{k_B T} = \frac{K_{\text{AF,IrMn}} \pi r_{\text{grain}}^2 t_{\text{IrMn}}}{k_B T} \approx 20 - 25 \quad (3)$$

is fulfilled (Boltzmann constant $k_B = 1.38 \times 10^{-23}$ J/K, temperature $T = 295$ K). With the AF grain radius $r_{\text{AF}} = 7.5$ nm (Refs. 22 and 25) and $K_{\text{AF,IrMn}} = 2 - 3 \times 10^5$ J/m³ (Refs. 22 and 45) this condition is matched for $t_{\text{IrMn}} = 1.50 - 2.35$ nm, covering $t_{\text{IrMn}} = 2.2$ nm where for the films the maximum tilt of AF-induced anisotropy is obtained and the coercivity reaches its maximum. Results for the fraction parameter $F = \sqrt{f^2(1-f)^2}$ derived from the fraction f of stable (or unstable) AF grains for an assumed grain size distribution are displayed in Fig. 10(b). An AF anisotropy of $K_{\text{AF,IrMn}} = 2.15 \times 10^5$ J/m³ and $T = 300$ K ($\Delta E/k_B T = 20$) was used for the calculations. The actual result is rather sensitive to the value of $K_{\text{AF,IrMn}}$ and a contribution to t_{IrMn} from magnetic dead layers due to layer intermixing has not been considered. Nevertheless, the estimation underpins the arguments given above. Moreover, the maximum of coercivity and anisotropy tilt coincide which has been directly related to interfacial magnetic frustrations⁴⁶ or a spin-glass state at the FM/AF interface.⁴⁷ For thicker values of t_{IrMn} additional effects from AF domains are suggested to contribute, so that AF stability and rotatable anisotropy effects still lead to a partly frustrated FM/AF interface, which is not considered in the calculations presented in Fig. 10(b). In addition, with the

$\langle 111 \rangle$ -fiber texture, even for solely stable AF magnetization a local variation of AF magnetization broadly varying along the direction of exchange bias occurs.

V. SUMMARY

In summary, we display direct evidence for strong deviation of collinear uniaxial and unidirectional coupling in polycrystalline ferromagnetic/antiferromagnetic bilayer structures. For low AF-layer thickness it leads to a uniaxial exchange anisotropy tilted up to $\pi/2$ relative to the ferromagnetic layer uniaxial anisotropy. For thicker AF layers, the skewed anisotropy contributions result in uneven reversal pathways. The misalignment between the imprinted FM

uniaxial and AF-induced exchange unidirectional anisotropy leads to an asymmetric reversal behavior that has been proven experimentally by integral and spatially resolved measurement techniques. The existence of tilted anisotropies, which form despite proper alignment of the magnetic field during deposition, is able to explain numerous published experimental data.^{25,32,33,48} Conditions for a symmetric reversal behavior are derived and confirmed experimentally by aligning the reversal field along the effective easy axis or easy direction of magnetization. The occurrence of tilted anisotropy contribution is highly relevant for applications in spintronics and for the fundamental comprehension of the FM/AF interaction. Presumably, magnetic frustration effects at the FM/AF interface similar to exchange-coupled FM/FM bilayers account for the found effects.

*j.mccord@ifw-dresden.de

- ¹P. Grünberg, R. Schreiber, Y. Pang, M. B. Brodsky, and H. Sowers, *Phys. Rev. Lett.* **57**, 2442 (1986).
- ²S. S. P. Parkin, *Phys. Rev. Lett.* **67**, 3598 (1991).
- ³M. Rühlig, R. Schäfer, A. Hubert, R. Mosler, J. Wolf, S. Demokritov, and P. Grünberg, *Phys. Status Solidi A* **125**, 635 (1991).
- ⁴D. E. Bürgler, D. M. Schaller, C. M. Schmidt, F. Meisinger, J. Kroha, J. McCord, A. Hubert, and H. J. Guntherodt, *Phys. Rev. Lett.* **80**, 4983 (1998).
- ⁵J. Slonczewski, *J. Magn. Magn. Mater.* **150**, 13 (1995).
- ⁶E. E. Fullerton, J. S. Jiang, M. Grimsditch, C. H. Sowers, and S. D. Bader, *Phys. Rev. B* **58**, 12193 (1998).
- ⁷J. Nogues and I. K. Schuller, *J. Magn. Magn. Mater.* **192**, 203 (1999).
- ⁸A. Berger, D. Margulies, and H. Do, *Appl. Phys. Lett.* **85**, 1571 (2004).
- ⁹A. Moser, A. Berger, D. Margulies, and E. Fullerton, *Phys. Rev. Lett.* **91**, 097203 (2003).
- ¹⁰V. K. Vlasko-Vlasov, U. Welp, J. S. Jiang, D. J. Miller, G. W. Crabtree, and S. D. Bader, *Phys. Rev. Lett.* **86**, 4386 (2001).
- ¹¹W. H. Meiklejohn and C. P. Bean, *Phys. Rev.* **102**, 1413 (1956).
- ¹²A. Berkowitz and K. Takano, *J. Magn. Magn. Mater.* **200**, 552 (1999).
- ¹³R. L. Stamps, *J. Phys. D* **33**, R247 (2000).
- ¹⁴F. Radu and H. Zabel, in *Magnetic Heterostructures, Advances and Perspectives in Spinstructures and Spintransport*, Springer Tracts in Modern Physics, edited by H. Zabel and S. D. Bader (Springer, New York, 2008), Vol. 227, pp. 97–183.
- ¹⁵A. P. Malozemoff, *J. Appl. Phys.* **63**, 3874 (1988).
- ¹⁶M. Stiles and R. McMichael, *Phys. Rev. B* **59**, 3722 (1999).
- ¹⁷N. C. Koon, *Phys. Rev. Lett.* **78**, 4865 (1997).
- ¹⁸U. Nowak, A. Misra, and K. D. Usadel, *J. Appl. Phys.* **89**, 7269 (2001).
- ¹⁹T. J. Moran, J. Nogués, D. Lederman, and I. K. Schuller, *Appl. Phys. Lett.* **72**, 617 (1998).
- ²⁰J. Nogués, D. Lederman, T. J. Moran, and I. K. Schuller, *Phys. Rev. Lett.* **76**, 4624 (1996).
- ²¹O. Petravic, Z.-P. Li, I. V. Roshchin, M. Viret, R. Morales, X. Batlle, and I. K. Schuller, *Appl. Phys. Lett.* **87**, 222509 (2005).
- ²²K. Steenbeck and R. Mattheis, *Phys. Rev. B* **75**, 134419 (2007).
- ²³H. Ohldag, A. Scholl, F. Nolting, E. Arenholz, S. Maat, A. T. Young, M. Carey, and J. Stöhr, *Phys. Rev. Lett.* **91**, 017203 (2003).
- ²⁴V. I. Nikitenko, V. S. Gornakov, A. J. Shapiro, R. D. Shull, K. Liu, S. M. Zhou, and C. L. Chien, *Phys. Rev. Lett.* **84**, 765 (2000).
- ²⁵J. McCord, R. Schäfer, R. Mattheis, and K. Barholz, *J. Appl. Phys.* **93**, 5491 (2003).
- ²⁶P. Blomqvist, K. M. Krishnan, and H. Ohldag, *Phys. Rev. Lett.* **94**, 107203 (2005).
- ²⁷D. T. Dekadjevi, A. Suvorova, S. Pogossian, D. Spenato, and J. Ben Youssef, *Phys. Rev. B* **74**, 100402 (2006).
- ²⁸B. Beckmann, U. Nowak, and K. Usadel, *Phys. Rev. Lett.* **91**, 187201 (2003).
- ²⁹J. Camarero, J. Sort, A. Hoffmann, J. M. Garcia-Martin, B. Dieny, R. Miranda, and J. Nogues, *Phys. Rev. Lett.* **95**, 057204 (2005).
- ³⁰D. Spenato, V. Castel, S. P. Pogossian, D. T. Dekadjevi, and J. B. Youssef, *Appl. Phys. Lett.* **91**, 062515 (2007).
- ³¹M. Fitzsimmons, P. Yashar, C. Leighton, I. Schuller, J. Nogues, C. Majkrzak, and J. Dura, *Phys. Rev. Lett.* **84**, 3986 (2000).
- ³²A. Kirilyuk, T. Rasing, H. Jaffres, D. Lacour, and F. Van Dau, *J. Appl. Phys.* **91**, 7745 (2002).
- ³³Y. G. Wang and A. K. Petford-Long, *J. Appl. Phys.* **92**, 6699 (2002).
- ³⁴A. Hubert and R. Schäfer, *Magnetic Domains: The Analysis of Magnetic Microstructures* (Springer, Heidelberg, NY, 1998).
- ³⁵S. Pogossian, D. Spenato, D. Dekadjevi, and J. Ben Youssef, *Phys. Rev. B* **73**, 174414 (2006).
- ³⁶H. Hoffmann, *IEEE Trans. Magn.* **4**, 32 (1968).
- ³⁷Z.-P. Li, O. Petravic, R. Morales, J. Olamit, X. Batlle, K. Liu, and I. K. Schuller, *Phys. Rev. Lett.* **96**, 217205 (2006).
- ³⁸T. R. Gao, D. Z. Yang, S. M. Zhou, R. Chantrell, P. Asselin, J. Du, and X. S. Wu, *Phys. Rev. Lett.* **99**, 057201 (2007).
- ³⁹P. Kappenberger, S. Martin, Y. Pellmont, H. J. Hug, J. B. Kortright, O. Hellwig, and E. E. Fullerton, *Phys. Rev. Lett.* **91**, 267202 (2003).
- ⁴⁰M. R. Fitzsimmons, B. J. Kirby, S. Roy, Z.-P. Li, I. V. Roshchin, S. K. Sinha, and I. K. Schuller, *Phys. Rev. B* **75**, 214412 (2007).

- ⁴¹M. Elhajal, B. Canals, R. Sunyer, and C. Lacroix, *Phys. Rev. B* **71**, 094420 (2005).
- ⁴²M. D. Stiles and R. D. McMichael, *Phys. Rev. B* **60**, 12950 (1999).
- ⁴³E. Fulcomer and S. H. Charap, *J. Appl. Phys.* **43**, 4190 (1972).
- ⁴⁴D. Choo, R. W. Chantrell, R. Lamberton, A. Johnston, and K. O'Grady, *J. Appl. Phys.* **101**, 09E521 (2007).
- ⁴⁵M. J. Carey, N. Smith, B. A. Gurney, J. R. Childress, and T. Lin, *J. Appl. Phys.* **89**, 6579 (2001).
- ⁴⁶C. Leighton, J. Nogues, B. J. Jonsson-Akerman, and I. K. Schuller, *Phys. Rev. Lett.* **84**, 3466 (2000).
- ⁴⁷F. Radu, A. Westphalen, K. Theis-Brohl, and H. Zabel, *J. Phys.: Condens. Matter* **18**, L29 (2006).
- ⁴⁸V. I. Nikitenko, V. S. Gornakov, L. M. Dedukh, Y. P. Kabanov, A. F. Khapikov, A. J. Shapiro, R. D. Shull, A. Chaiken, and R. P. Michel, *Phys. Rev. B* **57**, R8111 (1998).